Research Article | Vol. 27, No. 4 | 18 Feb 2019 | OPTICS EXPRESS A197
Optics EXPRESS

Optically addressing interaction of Mg/MgO plasmonic systems with hydrogen

YAEL GUTIERREZ,[1,2,5] MARIA M. GIANGREGORIO,[1] FABIO PALUMBO,[1] APRIL S. BROWN,[3] FERNANDO MORENO[2] AND MARIA LOSURDO[1,4]

[1]*Institute of Nanotechnology, CNR-NANOTEC, Via Orabona 4, 70126 Bari, Italy*
[2]*Department of Applied Physics, Universidad de Cantabria, Avda. Los Castros s/n 39005 Santander, Spain*
[3]*Department of Electrical Engineering, Duke University, Durham, NC 27708, USA*
[4]*maria.losurdo@cnr.it*
[5]*gvelay@unican.es*

Abstract: Magnesium-based films and nanostructures are being studied in order to improve hydrogen reversibility, storage capacity, and kinetics, because of their potential in the hydrogen economy. Some challenges with magnesium (Mg) samples are their unavoidable oxidation by air exposure and lack of direct *in situ real time* measurements of hydrogen interaction with Mg and MgO surfaces and Mg plasmonic nanoparticles. Given these challenges, the present article investigates direct interaction of Mg with hydrogen, as well as implications of its inevitable oxidation by real-time spectroscopic ellipsometry for exploiting the optical properties of Mg, MgH_2 and MgO. The direct hydrogenation measurements have been performed in a reactor that combines a remote hydrogen plasma source with an *in situ* spectroscopic ellipsometer, which allows optical monitoring of the hydrogen interaction and results in optical property modification. The hydrogen plasma dual use is to provide the hydrogen-atoms and to reduce barriers to heterogeneous hydrogen reactions.

1. Introduction

The interaction of magnesium, Mg, and its oxide, MgO, with hydrogen is of paramount importance for an hydrogen based economy due to magnesium hydride, MgH_2, which has high gravimetric and volumetric hydrogen densities of ρ_m = 7.6 wt % H and ρ_V = 110 kg H/m^3. Therefore, Mg has been the subject of intensive studies aimed at assessing its potential as a hydrogen storage system alone, doped, in alloys [1], and as nanostructures [2–4]. Nevertheless, critical issues related to hydrogen desorption temperature, higher than 300°C, sluggish kinetics of the hydrogen adsorption/desorption processes (as an example dehydrogenation from a 30 nm Mg layer in 19 h has been reported) [5] and fast Mg oxidation/corrosion by air exposure limit its hydrogen technology uptake. Therefore, Mg is being the subject of intensive studies aimed at understanding and overcoming those drawbacks.

Very recently the plasmonic properties of Mg nanodisks [6] have been exploited to investigate their hydrogenation/dehydrogenation processes in H_2, the so called "*hydrogenography*", based on the different dielectric function of metallic Mg and dielectric MgH_2 [7]. Indeed, most of those previous studies have reported the low activity of Mg in dissociating H_2, consequently Mg was covered or alloyed with Ti and Pd that were the catalytic metal inducing the dissociation of H_2; nevertheless, Mg-Pd-Ti alloying at interfaces and Pd, Ti themselves and TiH_2 [2] can affect the diffusion of hydrogen as well as the Mg hydrogenation kinetics and the optical response of the overall systems. Furthermore, Mg films and Mg nanoparticles samples are extremely reactive when they are exposed to air, water, and oxygen, and usually covered with a stable oxide $MgO/Mg(OH)_2$ nanometric layer [8]. Therefore, the first step of the interaction with hydrogen would involve the reduction of

#349866 https://doi.org/10.1364/OE.27.00A197
Journal © 2019 Received 2 Nov 2018; revised 9 Dec 2018; accepted 10 Dec 2018; published 13 Feb 2019

Optics EXPRESS

$MgO/Mg(OH)_2$; this interaction is also important considering that the hydrogen production by hydrolysis of Mg also produces $MgO/Mg(OH)_2$ (i.e. $Mg + H_2O \rightarrow MgO + H_2$). Therefore, any eco-friendly and practical hydrogen production system should consider recycling/reusing $MgO/MgOH_2$ to regenerate Mg/MgH_2, e.g. by cascading re-use or regeneration by H_2 plasma processes. Furthermore, another challenge is related to the air stability of the MgH_2 phase and the effect of this instability on the MgH_2 thermal decomposition, which has not been thoroughly defined [9].

Here the hydrogenation/de-hydrogenation processes of Mg film and plasmonic nanoparticles (NPs), a well as of MgO to evaluate its regeneration to Mg/MgH_2 and the air stability of MgH_2 are investigated via optical measurements by real time spectroscopic ellipsometry in the broad spectral range of 0.75 – 6.5 eV. The relevance of this optical study can also be gained considering that it allows monitoring any variation of Mg NPs localized surface plasmon resonance (LSPR) whose importance pops out from latest studies proposing Mg/MgH_2 nanostructure hydrogenation/dehydrogenation for plasmonic color displays [5,6]. Real time ellipsometric data are rationalized and modeled by electromagnetic simulations, whereas the chemical description of the $Mg/MgO/H_2$ interaction has been supported by Raman spectroscopy and X-ray photoelectron spectroscopy. Since comparable energy barriers of 1.05 and 1.33 eV have been reported for H_2 dissociation on the pure Mg and MgO surfaces, which are higher than the energy barrier of 0.39 eV for dissociation on catalyzed Pt/Pd-doped Mg [10], explaining the non-reactivity of Mg and MgO with molecular H_2, we have used atomic hydrogen produced by a remote H_2 plasma source to investigate the direct interaction of clean Mg with hydrogen to avoid any interference from primer Ti and capping Pd layers. Another benefit of the H_2 plasma approach is the reduction of MgO surface layer and penetration of energetic hydrogen into the subsurface region increasing the hydrogenation yield and thickness even for Mg thick films that have been in contact to air. This would add more flexibility to the implementation of Mg-hydrides formation routine operating a "plasma hydrogenation activation".

2. Experimental approach

Mg thick films (>100 nm) prepared by ion milling and Mg nanoparticles samples prepared by evaporating Mg under ultra-high-vacuum (UHV) 10^{-10} Torr system on an Al_2O_3 substrate at room temperature were used in this study.

The direct interaction with hydrogen was investigated in a reactor that combines a remote hydrogen plasma source with an *in situ* spectroscopic ellipsometer (UVISEL Horiba), allowing us to optical monitoring the hydrogen interaction and resulting modification of optical properties. Hydrogen exposure occurred at 1 Torr with a H_2 flow rate of 200 sccm, whereas atomic hydrogen was produced by a radiofrequency (r.f.) 13.56 MHz plasma at the low power of 50 W to study the direct interaction with H-atoms (since we are not using any Pd capping of Mg for the catalytic dissociation of H_2). The temperature during the hydrogenation/dehydrogenation was investigated in the range room 25-300°C, the latter being the MgH_2 dehydrogenation temperature [11]. Each sample was measured soon after the preparation, after their exposure to air, after the hydrogenation step *in situ* and finally after exposure to air. The experimental ellipsometric spectra of the complex pseudodielectric function, $\langle\varepsilon\rangle = \langle\varepsilon_r\rangle + i\langle\varepsilon_i\rangle$, were acquired in the range 1.5 – 6.5 eV with an energy resolution of 0.1 eV, and the kinetic data were acquired with a time resolution of 1 sec. The optical data were corroborated by chemical characterizations of Raman spectroscopy (LabRam Horiba) excited by a 532 nm laser, X-ray photoelectron spectroscopy (XPS) using a monochromatic Al Kα source (PHI 5400 VERSAPROBE) at a take-off angle of 45°, and atomic-force-microscopy (AFM) (AutoProbe CP, ThermoMicroscope).

In order to model the experimental results measured by ellipsometry in both thin films and nanoparticles, we have performed electromagnetic simulations in equivalent systems. In the case of the Mg thin films, spectral reflectance calculations in multilayer systems were

Optics EXPRESS

calculated using the transfer matrix method [12]. The formation of MgO and MgH_2 on Mg nanoparticles was modeled as multilayered spheres. The absorption efficiency of these type of nanoparticles were modeled using Mie theory [13]. The complex dielectric function, $\varepsilon = \varepsilon_r + i\varepsilon_i$, of Mg, MgO and MgH_2 used in the simulations were taken from different sources in the literature [12,13]. For the knowledge of the reader, the optical properties about the mentioned materials are shown in Figs. 1(a)-1(b). These dielectric function spectra are used for comparison with experimental pseudodielectric function spectra to understand qualitatively the findings.

3. Results and discussion

Figures 1(a)-1(b) shows a huge contrast in the dielectric function of the metallic Mg and dielectric MgO, as well as between Mg and the dielectric MgH_2. The layers of Mg after preparation and exposure to air for ex-situ measurements showed an oxide overlayer of approximately 25 nm; this can be read in Fig. 1(c) when comparing the dielectric function of pure Mg (red curves) with that of the air exposed film (blue curve): the oxide dielectric overlayer decreases $\langle\varepsilon_i\rangle$ and increases $\langle\varepsilon_r\rangle$ (less negative) reducing the metallic behavior. The oxide overlayer has been quantitatively estimated (25 nm) by analyzing the experimental pseudodielectric function spectra (blue curve) using the one-layer model sketched at the bottom of Fig. 1(e). Figure 1(b) shows that MgO and MgH_2 are both dielectric and differ mainly in the UV region above 5 eV, since the reported bandgap of 5.6 eV for MgH_2 [15] and of 7.8 eV for MgO [16], and in the refractive index being slightly higher for MgH_2 than MgO, e.g. 1.7 for MgO and 1.9 for MgH_2 at 2 eV. The consequence of this is by both kinetic ellipsometric data in Figs. 1(c)-1(d) and the transfer matrix method reflectance calculations in Figs. 1(e)-(g), is that when realistic Mg layers with the thin overlayer of MgO are exposed to atomic hydrogen, the reduction of MgO and the conversion of the outmost layer to MgH_2 results in small changes of the dielectric function in the visible range.

Specifically, Fig. 1(c) shows the pseudodielectric function $\langle\varepsilon\rangle = \langle\varepsilon_r\rangle + i\langle\varepsilon_i\rangle$ of the Mg layer before and after its exposure to a H_2 plasma. As reference the dielectric function of Mg from literature [14] is also plotted. By comparing the pseudodielectric function of the initial state of the layer sample with that of reference Mg, it can be inferred that the layer already has a ~25 nm oxide layer as indicated by the less negative real part of the dielectric function, $\langle\varepsilon_r\rangle$ and by the increased losses in the imaginary part, $\langle\varepsilon_i\rangle$. When exposed to the hydrogen plasma, the *in situ* ellipsometry monitoring shown in Fig. 1(d) indicates a decrease of $\langle\varepsilon_r\rangle$, which would be consistent with the reduction of MgO, and an increase of $\langle\varepsilon_i\rangle$, consistent with its transformation to MgH_2. Furthermore, the hydrogenation kinetics is saturating, because is limited by the slow diffusion of H-atoms to the reaction front by the already-grown "blocking" MgH_2 layer due to the much lower diffusion coefficient of hydrogen in the MgH_2 (eighth to ten order of magnitude lower) than in Mg. Specifically, the diffusion coefficient of H-atoms through forming MgH_2 layer is $D = 2.24 \times 10^{-21}$ m^2/s [17] which is orders of magnitude lower that H-atoms diffusion into Mg, ($D = 4.1 \times 10^{-13}$ m^2/sec) [18]. Therefore, most of Mg in the thick layers stays metallic and only the outmost layers (including the reduction of MgO) can be converted into MgH_2; this two-layer structure of the sample (as schematized at the bottom of Fig. 1(f)) -inner Mg-metal layer covered by the thin MgH_2 dielectric overlayer- explains also the still Drude behavior observed in Fig. 1(c), since the penetration depth of light is still probing both layer. By fitting the hydrogenated sample (orange spectrum in Fig. 1(c)) the two-layer model Al_2O_3-substrate/Mg [14]/MgH_2 [15] sketched at the bottom of Fig. 1(f), a thickness of 24 ± 1 nm has been estimated for the MgH_2 overlayer. Reflectance calculations under normal incidence of multilayer systems have been performed in order to evaluate the sensitivity of the optical response of a Mg layer grown on an Al_2O_3 substrate when MgO or MgH_2 layers are formed. We have modeled this situation by considering a Mg layer 50 nm thick on an Al_2O_3 substrate of infinite thickness. The formation of the MgO and MgH_2 has been taken into account by reducing the thickness of the Mg thin

Optics EXPRESS

film and by adding a layer of MgO or MgH_2 on top in order to keep the 50 nm thick of the system. Figures 1(f)-(g) shows the reflectance color maps as function of the photon energy and the MgO/MgH_2 layer thickness. The most significant differences can be spotted in the high energy range, where MgH_2 presents absorption and MgO has a loss less behavior. However, at lower energies both reflectance spectra are very similar no matter the thickness of the layer.

The real experimental situation is modeled in Fig. 1(g) where a 25 nm Mg layer on top of an Al_2O_3 substrate of infinite thickness is covered by a 25 nm MgO oxide which is converted progressively in MgH_2.

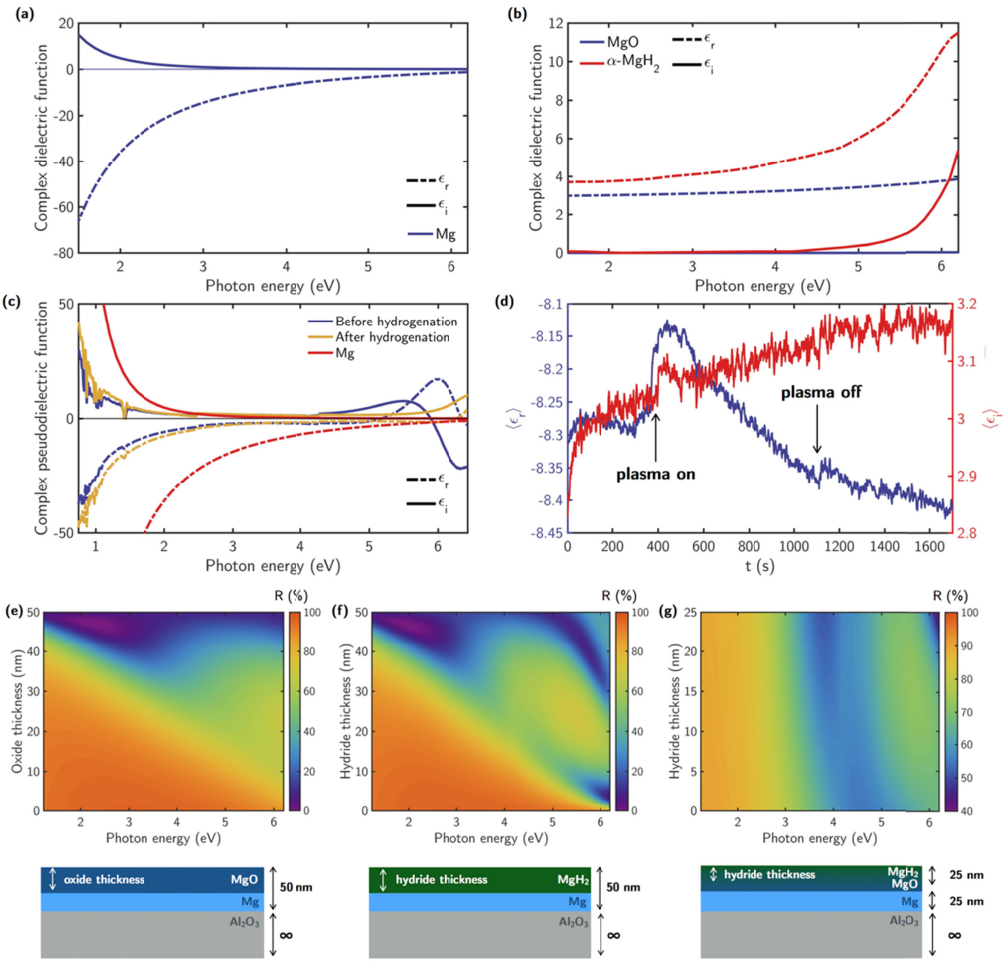

Fig. 1. Complex dielectric function ($\varepsilon = \varepsilon_r + i\varepsilon_i$) of (a) Mg [14] and (b) MgO [14] and α-MgH_2 [15]. (c) Experimental complex pseudodielectric function ($\langle\varepsilon\rangle = \langle\varepsilon_r\rangle + i\langle\varepsilon_i\rangle$) of a layer of Mg before (blue line) and after exposure (yellow line) to a H_2 plasma. As a reference, the dielectric function of Mg (red line) from Ref [14]. is also plotted (d) *In situ* ellipsometry monitoring at 2 eV of the real (blue line) and imaginary part (red line) of the pseudodielectric function during the H_2 plasma exposure. Reflectance color map as a function of the photon energy and the (e) Mg and (f,g) MgH_2 layer thickness under normal incidence. The multilayer configuration in each case is presented underneath.

The reflectance color map as a function of the photon energy and the thickness of the MgH_2 layer shows almost no difference as we go from MgO to a MgH_2 overlayer. The higher differences are found at the high energy regime, where the contrast in the optical constants

between the oxide and the hydride is bigger. This is consistent with the experimental values of the pseudodielectric constant before and after plasma exposure (see Fig. 1(c)).

In order to check if the self-limiting hydrogenation kinetics also applies to nanostructures, Mg nanoparticles (NPs) samples have been prepared. Figure 2(a) shows the real time evolution of the imaginary part of the pseudodielectric function for a sample constituted of closely packed Mg NPs grown on Al_2O_3. The spectra evolution clearly shows the appearance of localized surface plasmon resonances (LSPR) peaks (see arrows in Fig. 2(a)). Specifically, initially a LSPR peaked at 4.8 eV appears that stays constant in position and increases in amplitude with the increase of density of NPs whose diameter has been estimated by AFM to be 70 nm (see inset AFM Fig. 2(a)). With further deposition of Mg, an additional LSPR peak at lower energy appears, which red-shifts with increasing Mg deposition. It has been reported [7] that the Mg plasmon resonance can be tuned from the ultraviolet to the infrared; indeed in our case the red-shifting LSPR is due to the increasing size of agglomerates of the 70 nm nanoparticles as detailed by the AFM in inset in Fig. 2(a). Despite the presence of those plasmon resonances, no plasmon catalytic effect of the Mg LSPR has been observed on the H_2 dissociation when those NPs have been exposed to H_2. Indeed, Fig. 2(b) shows the complete damping of the Mg NPs LSPR by air exposure and consequent oxidation of the Mg NPs, demonstrating one of the limits of the Mg NPs in plasmonics, which is the full oxidation of the Mg NPs with time. Indeed, when the lower $\langle\varepsilon_i\rangle$ spectrum in Fig. 2(b) was recorded, XPS showed mainly the MgO component in the Mg2p photoelectron core level (see Fig. 3(a)), indicating that most of the NPs were oxidized. This is consistent with the electromagnetic modeling and absorption efficiency, Q_{abs}, of a multilayer Mg-core/MgO-shell sphere, with the thickness of the shell increases consuming all the metal content in the NP, shown in Fig. 2(e). For the Mg-core the Mg dielectric function from Ref [14] has been used, while for the MgO-shell or the outer MgH_2-shell the MgO and MgH_2 respective dielectric functions from Ref [15]. have been used. Since the surrounding media of our particles are the air and the substrate Al_2O_3, the spheres have been placed in an effective surrounding medium of refractive index $n_{med} = 1.5$ to consider the effect of the substrate, the air and the rest of the aggregates (see AFM images in Fig. 2(a)). The refractive index of the effective medium is defined as $n_{med} = (1- \gamma)\cdot n_{air} + \gamma \cdot n_{subs}$ [19], where the substrate refractive index and that of the rest of particles has been considered in n_{subs} with a value of 1.7, and the weight $\gamma = 0.7$. The parameter γ can be interpreted as the fraction of the volume surrounding the particle with refractive index 1.7.

Figure 2(e) shows the absorption efficiency, Q_{abs}, color map of Mg-MgO core-shell as function of the photon energy and of the MgO shell thickness. It can be seen how the localized plasmon peaks visible in Q_{abs} due to the Mg core are completely quenched when the NP is fully MgO. This is expected since the imaginary part of its dielectric constant is zero in all the analyzed spectral range. Figure 2(f) shows the case of a growing MgH_2 shell on a Mg nanoparticle. In this case, below ≈5 eV ($\varepsilon_2(MgH_2) = 0$), the Q_{abs} color map shows the same behavior as in the case of the MgO shell: the localized plasmon peaks are quenched as the shell of the hydride increases. However, above 5 eV, an absorption band appear due to the losses introduced by the MgH_2 shell. Thus, the growing of either a MgO or a MgH_2 shell can be clearly distinguished in the high energy range. When mimicking the real situation, the conversion of the MgO shell into a MgH_2 upon H_2 plasma exposure (see Fig. 3(g)), the main differences in the Q_{abs} color map as function of the photon energy and the hydride layer thickness can be seen again at energies above 5 eV. When metallic core is covered by the pure oxide shell, the absorption at high energies is zero. However, as the outer layers of oxide become to be replaced by the hydride, the values of Q_{abs} start to increase reaching a maximum when the oxide is completely converted in the hydride.

Therefore, even the hydrogenation of the Mg NPs without any capping has to consider as first the reduction of the native oxide overlayer. Figure 2(c) shows the real time kinetics for the variation of both the real, $\langle\varepsilon_r\rangle$, and imaginary part, $\langle\varepsilon_i\rangle$, of the pseudodielectric function,

Optics EXPRESS

during exposure to H-atoms; the increase in $\langle\varepsilon_r\rangle$ and decrease in $\langle\varepsilon_i\rangle$ are observed, as also indicated by the spectra in Fig. 2(d), which are consistent with MgH_2 formation, similarly to what reported by Sterl et al. [6] until again a saturation value is achieved which corresponds to the max uptake of hydrogen from the Mg NPs; this saturation level does not change even increasing further the temperature or H_2 pressure during the hydrogenation.

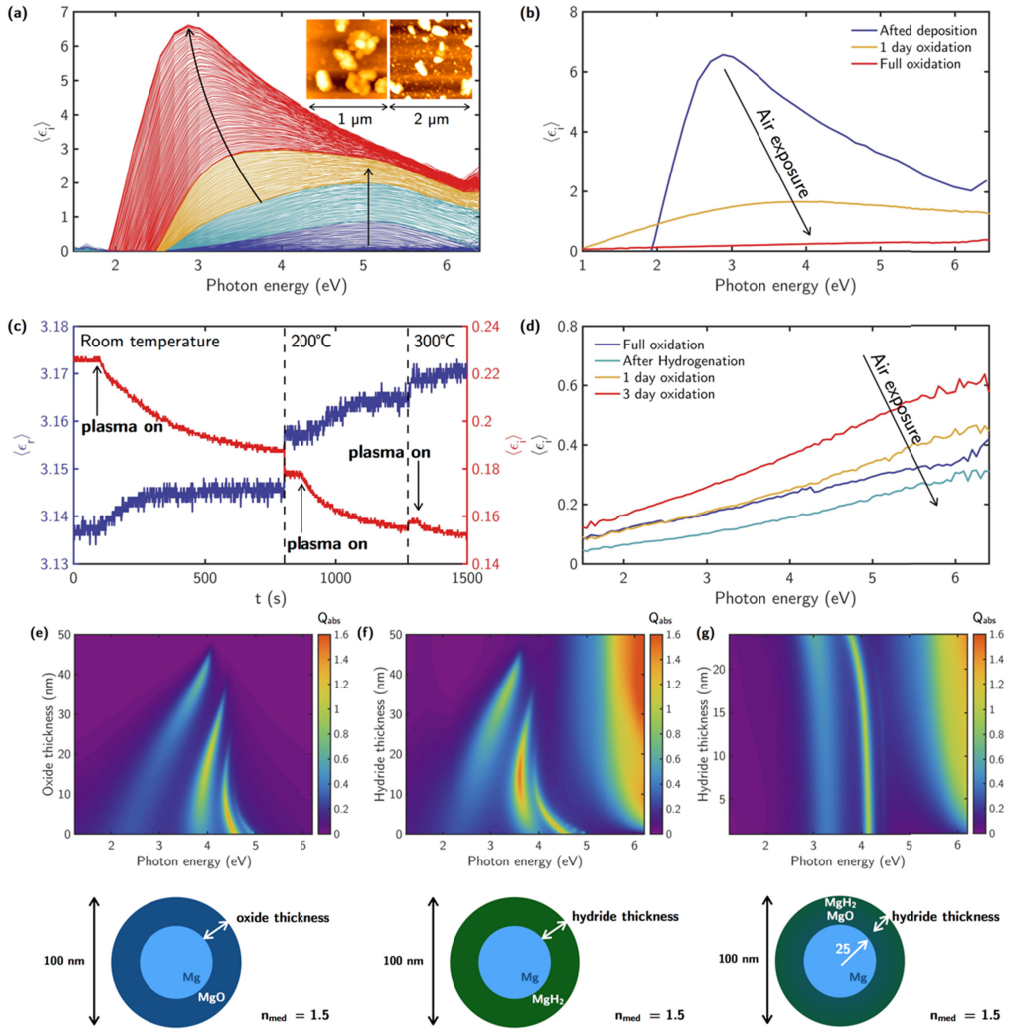

Fig. 2. (a) Real time evolution of the imaginary part of the pseudodielectric function ($\langle\varepsilon\rangle = \langle\varepsilon_r\rangle + i\langle\varepsilon_i\rangle$) for Mg NPs grown on Al_2O_3. With arrows are indicated the evolution in time of the two LSPRs. As inset are shown AFM images of the samples under study. (b) Mg LSPR damping by air exposure and oxidation. (c) *In situ* ellipsometry monitoring at 3 eV of the real (blue line) and imaginary part (red line) during the H_2 plasma exposure at different temperatures. (e) Experimental pseudodielectric function of a sample of oxidized Mg NPs before and after hydrogenation, and its evolution after air exposure. Absorption efficiency color map as a function of the photon energy and the (e) Mg and (f,g) MgH_2 shell thickness. The core-shell configuration in each case is presented underneath. The NPs are placed in a medium with refractive index n_{med} = 1.5 to take into account the effect of the substrate and the rest of the NPs in the sample.

Interestingly, no variation is observed when the H_2 is stopped, indicating that the hydrogenated state of the particles remains fixed when in N_2, Ar or UHV, i.e., no hydrogen desorption occurs at T < 300 °C, when H_2 is dropped off the surrounding atmosphere.

Optics EXPRESS

Contrarily, as soon as the hydrogenated NPs are exposed to air, in a few hours the $\langle\varepsilon_i\rangle$ spectrum increases again (see Fig. 2(c)). Those modifications of the optical spectra can be rationalized on the basis of the XPS results in Fig. 3. Specifically, the increase of $\langle\varepsilon_i\rangle$ of the air exposed MgH_2 can be ascribed to $Mg(OH)_2$ that forms rapidly on the MgH_2 surface when contacting with air humidity [9], as well as the XPS O1s spectra shows mainly the MgO (including Al_2O_3 from the substrate) component before hydrogenation while for the hydrogenated sample in addition to the Al_2O_3.

XPS spectra of the Mg photoelectron core level and of the MgKLL Auger line are also reported in Fig. 3. Here although the MgO and MgH_2 components cannot be separated in the Mg2p photoelectron core level, before hydrogenation only one symmetric component at 51.4 eV is observed ascribed to MgO, whereas upon hydrogenation a shift of the peak to 50.8 eV consistent with MgH_2, a lower binding energy component at 49.3 eV due to metallic Mg appears, indicating that the MgO was reduced and the hydrogenation did not completely hydrogenated all sample, probably because of the barrier effect of the already formed MgH_2 layer. Furthermore, the appearance of the tail peak in Mg2p due to $Mg(OH)_2$ also indicates that the air exposed MgH_2 is not stable and forms hydroxide. This is also supported by the O1s photoelectron core level that also shows a main component at 531.4 eV due to MgO before hydrogenation and to the Al_2O_3 substrate and a component at 533.2 eV of hydroxide $Mg(OH)_2$ after hydrogenation. Also the high resolution MgKLL Auger peak of Mg before and after hydrogenation indicates the presence of metallic Mg, a more prominent Mg bulk plasmon peak, and the formation of hydroxide $Mg(OH)_2$.

The newly formed phase of MgH_2 upon hydrogenation has been confirmed by the Raman analysis (Fig. 3(b)), showing after hydrogenation peaks of the B_{1g}, E_g and A_{1g} phonon modes characteristics of α-MgH_2, whereas before hydrogenation only very broad peak of nanocrystalline/amorphous MgO was observed.

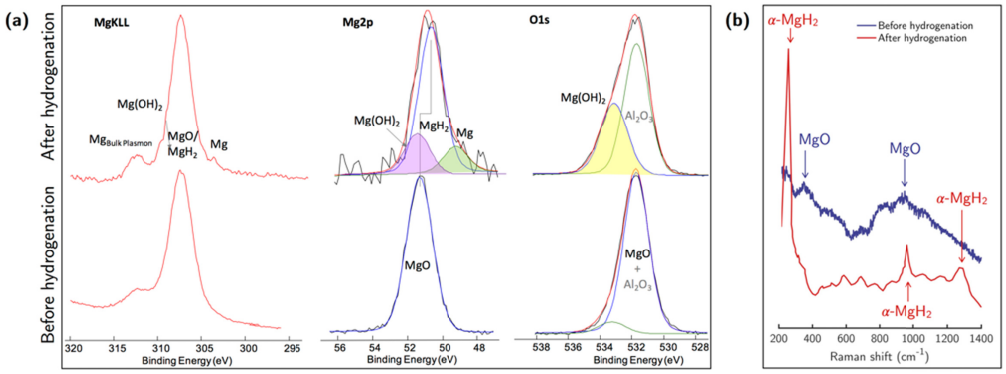

Fig. 3. (a) XPS spectra of the MgKLL Auger line, and of the Mg2s and O1s photoelectron core level of the Mg NPs sample before and after hydrogenation, both after air exposure for 5h. (b) Raman spectra of Mg nanoparticles before and after H_2 plasma exposure.

The present optical and chemical results are consistent with the heterolytic -Mg(H)-O(H)- chemisorption of hydrogen on MgO [20,21], as schematized in Fig. 4, which produces hydride and hydroxy groups which are partially reversible upon evacuation, as well as the desorption H_2O leaving some Mg sites that can be further hydrogenated or remain as unsaturated Mg, as also evidenced by the XPS.

Optics EXPRESS

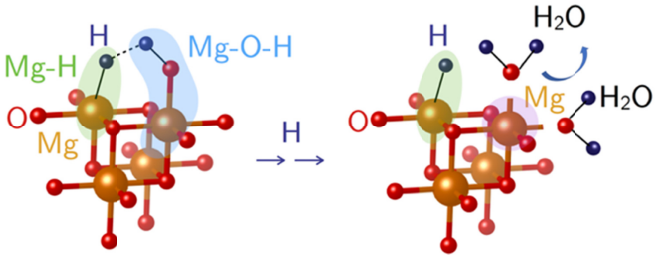

Fig. 4. Scheme of the heterolytic -Mg(H)-O(H)- chemisorption of hydrogen on MgO surfaces.

4. Summary

In summary, the *in situ real time* ellipsometry study of the interaction of hydrogen with Mg surfaces and Mg plasmonic nanoparticles realistically covered by a thin overlayer of MgO has revealed the self-limiting character of the Mg hydrogenation kinetics due to the reduction of the oxide layer, in a first step, and to the conversion of the outmost layer into MgH_2, indicating that the MgO into MgH_2 conversion and subsequent Mg hydrogenation is limited by the slow diffusion of the hydrogen atoms in the growing "blocking" MgH_2 layer. The MgH_2 also oxidizes to some extent by air exposure forming the hydroxide $Mg(OH)_2$.

Furthermore, we have demonstrated that Mg NPs, although they present a tunable plasmonic response in a wide spectral, their use is limited by the complete quenching of the LSPRs when exposed to air due to the complete oxidation of the nanoparticle, if a capping layer is not used.

Funding

European Commission under the H2020 grant TWINFUSYON (GA692034). Army Research Laboratory under Cooperative Agreement Number W911NF-17-2-0023. SODERCAN (Sociedad para el Desarrollo de Cantabria) through the Research Vicerrectorate of the University of Cantabria.

Acknowledgments

Y.G. wants to thank the University of Cantabria for her FPU grant.

References

1. H. Shao, L. He, H. Lin, and H.-W. Li, "Progress and Trends in Magnesium-Based Materials for Energy-Storage Research: A Review," Energy Technol. (Weinheim) **6**(3), 445–458 (2018).
2. L. Pasquini, "The Effects of Nanostructure on the Hydrogen Sorption Properties of Magnesium-Based Metallic Compounds: A Review," Crystals (Basel) **8**(2), 106 (2018).
3. X. Yu, Z. Tang, D. Sun, L. Ouyang, and M. Zhu, "Recent advances and remaining challenges of nanostructured materials for hydrogen storage applications," Prog. Mater. Sci. **88**, 1–48 (2017).
4. T. Sadhasivam, H.-T. Kim, S. Jung, S.-H. Roh, J.-H. Park, and H.-Y. Jung, "Dimensional effects of nanostructured Mg/MgH 2 for hydrogen storage applications: A review," Renew. Sustain. Energy Rev. **72**, 523–534 (2017).
5. X. Duan and N. Liu, "Scanning Plasmonic Color Display," ACS Nano **12**(8), 8817–8823 (2018).
6. F. Sterl, N. Strohfeldt, R. Walter, R. Griessen, A. Tittl, and H. Giessen, "Magnesium as Novel Material for Active Plasmonics in the Visible Wavelength Range," Nano Lett. **15**(12), 7949–7955 (2015).
7. F. Sterl, H. Linnenbank, T. Steinle, F. Mörz, N. Strohfeldt, and H. Giessen, "Nanoscale Hydrogenography on Single Magnesium Nanoparticles," Nano Lett. acs.nanolett.8b01277 (2018).
8. M. Santamaria, F. Di Quarto, S. Zanna, and P. Marcus, "Initial surface film on magnesium metal: A characterization by X-ray photoelectron spectroscopy (XPS) and photocurrent spectroscopy (PCS)," Electrochim. Acta **53**(3), 1314–1324 (2007).
9. V. D. Dobrovolsky, O. Y. Khyzhun, A. K. Sinelnichenko, O. G. Ershova, and Y. M. Solonin, "XPS study of influence of exposure to air on thermal stability and kinetics of hydrogen decomposition of MgH 2 films obtained by direct hydrogenation from gaseous phase of metallic Mg," J. Electron Spectrosc. Relat. Phenom. **215**, 28–35 (2017).
10. G. Wu, J. Zhang, Y. Wu, Q. Li, K. Chou, and X. Bao, "The effect of defects on the hydrogenation in Mg (0001) surface," Appl. Surf. Sci. **256**(1), 46–51 (2009).

Optics EXPRESS

11. B. Sakintuna, F. Lamaridarkrim, and M. Hirscher, "Metal hydride materials for solid hydrogen storage: A review," Int. J. Hydrogen Energy **32**(9), 1121–1140 (2007).
12. M. Born, E. Wolf, A. B. Bhatia, P. C. Clemmow, D. Gabor, A. R. Stokes, A. M. Taylor, P. A. Wayman, and W. L. Wilcock, *Principles of Optics* (Cambridge University, 1999).
13. C. F. Bohren and D. R. Huffman, eds., *Absorption and Scattering of Light by Small Particles* (Wiley-VCH Verlag GmbH, 1998).
14. E. D. Palik, *Handbook of Optical Constants of Solids* (Academic, 1998).
15. J. Isidorsson, H. Arwin, and R. Griessen, "Optical properties of MgH_2 measured in situ in a novel gas cell for ellipsometry/spectrophotometry," 1–15 (2018).
16. O. E. Taurian, M. Springborg, and N. E. Christensen, "Self-consistent electronic structures of MgO and SrO," Solid State Commun. **55**(4), 351–355 (1985).
17. J. Čermák and L. Král, "Hydrogen diffusion in Mg–H and Mg–Ni–H alloys," Acta Mater. **56**(12), 2677–2686 (2008).
18. J. L. Anchell, K. Morokuma, and A. C. Hess, "An electronic structure study of H 2 and CH 4 interactions with MgO and Li□doped MgO clusters," J. Chem. Phys. **99**(8), 6004–6013 (1993).
19. A. Curry, G. Nusz, A. Chilkoti, and A. Wax, "Substrate effect on refractive index dependence of plasmon resonance for individual silver nanoparticles observed using darkfield microspectroscopy," Opt. Express **13**(7), 2668–2677 (2005).
20. Z. Song, H. Hu, H. Xu, Y. Li, P. Cheng, and B. Zhao, "Heterolytic dissociative adsorption state of dihydrogen favored by interfacial defects," Appl. Surf. Sci. **433**, 862–868 (2018).
21. S. Coluccia, F. Boccuzzi, G. Ghiotti, and C. Morterra, "Infrared study of hydrogen adsorption on MgO, CaO and SrO. Possible mechanism in promoting O–2 formation," J. Chem. Soc. Faraday Trans. 1 Phys. Chem. Condens. Phases **78**, 2111 (1982).